


# Ion Transport and Molecular Organization Are Coupled in Polyelectrolyte-Modified Nanopores

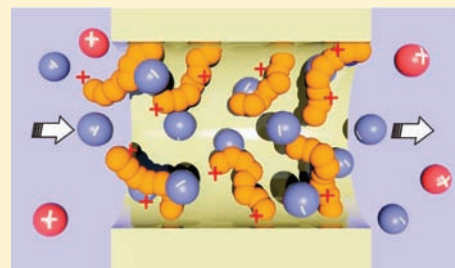
Mario Tagliazucchi,<sup>†</sup> Yitzhak Rabin,<sup>†,‡</sup> and Igal Szleifer<sup>\*,†</sup>

<sup>†</sup>Department of Biomedical Engineering, Department of Chemistry and Chemistry of Life Processes Institute, Northwestern University, Evanston, Illinois 60208, United States

<sup>‡</sup>Department of Physics and Institute for Nanotechnology and Advanced Materials, Bar-Ilan University, Ramat-Gan, 52900, Israel

 Supporting Information

**ABSTRACT:** Chemically modified nanopores show a strong and nontrivial coupling between ion current and the structure of the immobilized species. In this work we study theoretically the conductance and structure in polymer modified nanopores and explicitly address the problem of the coupling between ion transport and molecular organization. Our approach is based on a nonequilibrium molecular theory that couples ion conductivity with the conformational degrees of freedom of the polymer and the electrostatic and nonelectrostatic interactions among polyelectrolyte chains, ions, and solvent. We apply the theory to study a cylindrical nanopore between two reservoirs as a function of pore diameter and length, the length of the polyelectrolyte chains, their grafting density, and whether they are present or not on the outer reservoir walls. In the very low applied potential regime, where the distribution of polyelectrolyte and ions is similar to that in equilibrium, we present a simple analytical model based on the combination of the different resistances in the system that describes the conductance in excellent agreement with the calculations of the full nonequilibrium molecular theory. On the other hand, for a large applied potential bias, the theory predicts a dramatic reorganization of the polyelectrolyte chains and the ions. This reorganization results from the global optimization of the different interactions in the system under nonequilibrium conditions. For nanopores modified with long chains, this reorganization leads to two interesting physical phenomena: (i) control of polyelectrolyte morphology by the direction and magnitude of ion-fluxes and (ii) an unexpected decrease in system resistance with the applied potential bias for long chains due to the coupling between polyelectrolyte segment distribution and ion currents.



## 1. INTRODUCTION

Natural and man-made pores and channels of nanoscale dimensions display unique ionic conductivity behavior, not observed in their microscale counterparts.<sup>1–5</sup> These new properties emerge when channels are narrowed to the characteristic length scale of the electrostatic interactions (the Debye length). On the other hand, nanopores modified with supramolecular chemical species (such as polyelectrolyte brushes<sup>6</sup>) have dimensions that not only are similar to the range of the electrostatic interactions but are also similar to the molecular size of the tethered macromolecules. The competition between these length scales creates interesting possibilities for the creation of stimuli responsive gates and ion channels<sup>6–13</sup> and for the fundamental understanding of the interplay between molecular organization and charge transport in nanoconfined environments.

Very recently, nanochannels and nanopores modified by synthetic<sup>9,10,12,14–17</sup> and biological<sup>11,13,18–21</sup> polymers and polyelectrolytes have been prepared, and the conductance at the single pore level has been measured. Polyelectrolyte-modified nanopores are very appealing for the design of stimuli-responsive ion gates because grafted macromolecules will affect the transport properties, but also because the conformations and properties of the confined molecules will be modified by the ionic

currents flowing through the system. As an interesting example, ion current rectification in DNA-modified conical nanopores was proposed to arise from the electrophoretic insertion/expulsion of grafted DNA into/from the mouth of the pore as a response to the applied bias.<sup>22</sup>

Our understanding of the systems described above is limited by the fact that the state of the art theoretical descriptions of ionic conductance in nanopores (based on the Nernst–Planck–Poisson (NPP) equations<sup>1</sup>) neglect the molecular details of the macromolecular structures inside the pore and the free species in solution, as well as their response to and their impact on the ionic fluxes through the system. Namely, the NPP approach considers only the electrostatic interactions in the system because it assumes that all the species are point ions and neglects excluded volume and other non-Coulomb interactions. An improved theoretical picture of the conductance of chemically modified nanofluidic devices is important to understand and design applications in diverse areas, such as energy transduction,<sup>23,24</sup> analytical chemistry,<sup>25–27</sup> ionic circuits,<sup>28</sup> or proton exchange membranes.<sup>29</sup>

Received: July 8, 2011

Published: September 25, 2011

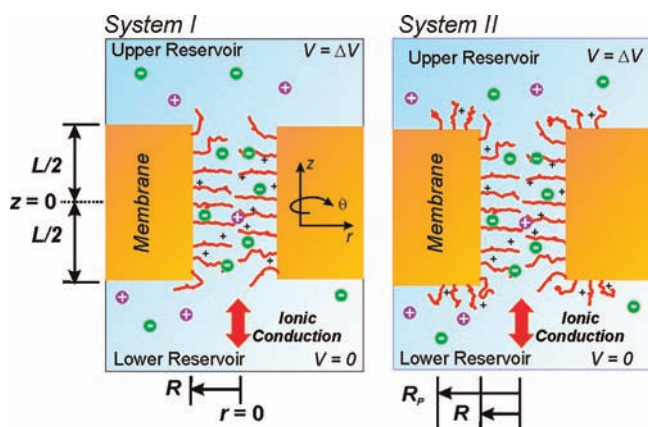


**Figure 1.** Scheme of the systems under study: a single cylindrical pore of radius  $R$  in a membrane of thickness  $L$ . The membrane separates two infinite reservoirs containing identical aqueous solutions of a 1:1 salt; more specifically, the solutions contain cations (C), anions (A), and water molecules. The inner walls of the pore (system I) or both the inner and outer walls up to a radius  $R_p$  (system II) are modified with polybase chains at a constant grafting density  $\rho_G$ . Each chain bears  $N$  monomers, each one having a charge  $f$ . Ion transport in the system results from applying an electrostatic potential difference  $\Delta V$  between the bulk solutions of the reservoirs (i.e., by means of reversible electrodes). We adopt the convention  $V \equiv 0$  for the lower reservoir.

In this work we present the first theoretical description of steady-state ionic fluxes through short nanopores modified with supramolecular structures. Our theoretical framework combines a previously developed molecular theory that is very well suited to describe soft materials at interfaces<sup>30–34</sup> with a description of the molecular transport in the system. The theory can predict the off-equilibrium molecular organization of the system and its transport properties, such as the current–potential ( $I$  vs  $\Delta V$ ) curves. Moreover, it provides a link between these two properties, and thus it can lead to design principles for chemically modified nanofluidic elements.

For large applied bias and short pores, we show that ionic currents strongly couple to polyelectrolyte conformations and ion distribution. This complex molecular organization out of equilibrium is predicted to produce nonohmic behaviors. For instance, the coupling between polyelectrolyte reorganization and ion currents can lead to an increase in the pore conductance with the applied potential bias. For small applied potentials, we present a simple model to describe the conductance and validate it using the full nonequilibrium molecular theory.

The systems studied in the present work are shown in Figure 1. System I consists in a single nanopore of radius  $R$  and length  $L$  connecting two reservoirs. Both reservoirs contain the same salt solution, composed of solvent (water), cations, and anions. Polyelectrolyte chains of length  $N$  and a fixed (positive) charge per monomer  $f$  are end-grafted to the inner walls of the pore with a surface density  $\rho_G$ . Our model system corresponds to a strong (nonregulating) polyelectrolyte; several examples of these polyelectrolytes have been used in single nanopores or nanopore membranes, such as poly(sulfonates),<sup>29,35</sup> DNA,<sup>18,19,22</sup> or poly-(quaternary amines).<sup>36</sup> System II is similar to system I, but chains are also grafted to the outer walls (also with a surface density  $\rho_G$ ) up to a distance  $R_p$  from the axis of the pore. Ionic currents result from applying an electrostatic potential bias  $\Delta V$  between the bulk solutions at the reservoirs (i.e., by means of two reversible electrodes).

## 2. THEORY

We present in this section a concise description of the nonequilibrium theory. Its formulation follows the ideas of the local equilibrium approximation,<sup>37,38</sup> namely, we assume that the thermodynamic variables in the system can be defined locally and the equilibrium functional relationships among them are still valid out of equilibrium. These ideas have been previously used to couple transport equations and density functional theories to describe fluxes in solvent mixtures,<sup>39</sup> ion transport in bare nanopores,<sup>40</sup> protein adsorption on bare and polymer modified surfaces,<sup>41–43</sup> etc. In one of these examples, the theoretical predictions for the steady-state transport in a simple two-component system were found to be in excellent agreement with nonequilibrium molecular dynamics simulations.<sup>39</sup>

The presence of chemical potential differences or gradients within a system drives mass fluxes from high chemical potential to low chemical potential regions. In our system, chemical potential differences for the ions arise from the externally applied bias. Therefore, we start by writing down an expression for the mass fluxes in the system as a function of the chemical potential gradients, which we will consider within the linear response regime. Neglecting the cross-terms associated with the off-diagonal elements in the Onsager coefficient matrix we have,

$$J_i(\mathbf{r}, t) = -D_i \rho_i(\mathbf{r}, t) \nabla \beta \mu_i(\mathbf{r}, t) \quad (1)$$

where  $D_i$  is the diffusion coefficient of the species  $i$  ( $i = A$  and  $C$ ),  $\mu_i(\mathbf{r}, t)$  and  $\rho_i(\mathbf{r}, t)$  are the chemical potential and the density of the species  $i$  at  $\mathbf{r}$  and time  $t$ , respectively, and  $\beta = 1/k_B T$ . Equation 1 describes the flux of the average densities and is equivalent to the general expression previously derived from the Langevin equations of motion for a system of colloidal particles in a bath.<sup>44,45</sup> The chemical potential in eq 1 is defined in analogy to the equilibrium potential:

$$\beta \mu_i(\mathbf{r}, t) = \frac{\delta \beta W}{\delta \rho_i(\mathbf{r}, t)} \quad (2)$$

where  $W$  is the free energy of the system.

For any system, we can separate the ideal from the nonideal contributions to the chemical potential in the form

$$\beta \mu_i(\mathbf{r}, t) = \ln(\rho_i(\mathbf{r}, t) v_w) + \beta U_i^{\text{mf}}(\mathbf{r}, t) \quad (3)$$

where the first term on the right-hand side is the ideal contribution to the chemical potential arising from the translational entropy and  $U_i^{\text{mf}}(\mathbf{r}, t)$ , the potential of mean force for the species  $i$ , represents the nonideal contribution that arises from intramolecular interactions and the presence of external fields. This nonideal contribution is a position-dependent activity coefficient,  $\phi_i(\mathbf{r}, t) = \exp(-\beta U_i^{\text{mf}}(\mathbf{r}, t))$ . Combining eqs 1 and 3 yields

$$J_i(\mathbf{r}, t) = -D_i \nabla \rho_i(\mathbf{r}, t) - D_i \rho_i(\mathbf{r}, t) \nabla \beta U_i^{\text{mf}}(\mathbf{r}, t) \quad (4)$$

This expression shows that the diffusion in the system can be separated into an ideal diffusion term, which is entropic in origin and gives rise to Fick's first law (first term) and a nonideal contribution (second term), as has been shown for the adsorption of proteins on surfaces with grafted polymers.<sup>42,43,46</sup>

The calculation of the chemical potential in eq 2 requires an expression for  $W$  that in our case is based on a previously reported molecular theory for polyelectrolytes grafted to curved surfaces<sup>31,32</sup> adapted here to describe a short pore connecting two reservoirs.<sup>47</sup> The molecular theory explicitly accounts for

the shape, charge, size, and conformational degrees of freedom of all the species in the system and the relevant inter- and intramolecular interactions. The predictions of the theory have been found to properly describe structural, thermodynamic, and functional properties of charged polyelectrolytes as compared with experimental observations.<sup>32–34,48</sup> In particular, we have shown that the theory is able to predict the pH-dependent conductance of polyelectrolyte-modified long nanochannels in excellent agreement with the experiments.<sup>32</sup>

We start by writing down an expression for the system Helmholtz free energy,  $F$ , as a functional of the probability of each conformation  $\alpha$  at each grafting position,  $P_P(\mathbf{r}(s), \alpha, t)$ ; the density of the free molecular species in solution at  $\mathbf{r}$  and time  $t$ ,  $\rho_i(\mathbf{r}, t)$  where  $i = w, C, A$  for water, cations, and anions and the electrostatic potential at  $\mathbf{r}$  and time  $t$ ,  $\psi(\mathbf{r}, t)$ . The total free energy is given by

$$\begin{aligned} \beta F = & \int \rho_w(\mathbf{r}, t) [\ln(\rho_w(\mathbf{r}, t)v_w) - 1] d\mathbf{r} + \int \rho_A(\mathbf{r}, t) [\ln(\rho_A(\mathbf{r}, t)v_w) - 1] d\mathbf{r} \\ & + \int \rho_C(\mathbf{r}, t) [\ln(\rho_C(\mathbf{r}, t)v_w) - 1] d\mathbf{r} \\ & + \rho_G \int \sum_{\alpha} P_P(\mathbf{r}(s), \alpha, t) \ln(P_P(\mathbf{r}(s), \alpha, t)) ds \\ & + \int \left[ \langle \rho_Q(\mathbf{r}, t) \rangle \beta \psi(\mathbf{r}, t) - \frac{1}{2} \varepsilon (\nabla \psi(\mathbf{r}, t))^2 \right] d\mathbf{r} \end{aligned} \quad (5)$$

where  $\varepsilon$  is the dielectric constant (assumed to be position and time independent),  $v_i$  is the molecular volume of the species  $i$ ,  $\langle \rho_Q(\mathbf{r}, t) \rangle$  is the average total charge density at  $\mathbf{r}$  and time  $t$ , and  $\mathbf{r}(s)$  is a parametrization of the surface where the polyelectrolytes are grafted. The first three terms in eq 5 account for the translational (mixing) entropy of the mobile species, the fourth term is the total conformational entropy of the polymer chains, and the last term represents the electrostatic contributions to the free energy. Repulsive interactions among molecular species in the system are modeled as excluded volume repulsions and are taken into account by a packing constraint at each  $\mathbf{r}$ :

$$\rho_A(\mathbf{r}, t)v_A + \rho_C(\mathbf{r}, t)v_C + \rho_w(\mathbf{r}, t)v_w + \langle \phi_P(\mathbf{r}, t) \rangle = 1 \quad (6)$$

where  $\langle \phi_P(\mathbf{r}, t) \rangle$  is the polyelectrolyte volume fraction at  $\mathbf{r}$  and time  $t$ . To enforce this requirement, we consider the potential  $W$ , which is a Legendre transform of  $F$ ,

$$\beta W = \beta F + \int \beta \pi(\mathbf{r}, t) \left[ \sum_{i=A, C, w} \rho_i(\mathbf{r}, t)v_i + \langle \phi_P(\mathbf{r}, t) \rangle - 1 \right] d\mathbf{r} \quad (7)$$

where  $\pi(\mathbf{r}, t)$  is the Lagrange multiplier associated with the excluded volume interactions. In equilibrium, this field introduces an excluded volume contribution to the chemical potential of the solvent that balances that arising from the local solvent density, and therefore  $\pi(\mathbf{r}, t)$  is a position-dependent osmotic pressure.<sup>49</sup>

We then insert eq 7 into eq 2 to get

$$\beta \mu_i(\mathbf{r}, t) = \ln(\rho_i(\mathbf{r}, t)v_w) + v_i \beta \pi(\mathbf{r}, t) + q_i \beta \psi(\mathbf{r}, t) \quad (8)$$

where  $q_i$  is the charge of the species  $i$ . Substituting eq 8 into eq 1 gives us an explicit expression for the mass fluxes of the ions in the system:

$$\begin{aligned} \mathbf{J}_i(\mathbf{r}, t) = & -D_i \nabla \rho_i(\mathbf{r}, t) - D_i \rho_i(\mathbf{r}, t) q_i \nabla \beta \psi(\mathbf{r}, t) \\ & - D_i \rho_i(\mathbf{r}, t) v_i \nabla \beta \pi(\mathbf{r}, t) \end{aligned} \quad (9)$$

Comparison of eqs 8 and 9 with eqs 3 and 4 reveals that  $\beta U_i^{\text{mf}}(\mathbf{r}, t) = \beta \pi(\mathbf{r}, t) v_i + q_i \beta \psi(\mathbf{r}, t)$ , and therefore in our case the potential of mean-force has contributions from the osmotic pressure, which represent intermolecular repulsive interactions and the electrostatic potential. However, since the electrostatic potential and the osmotic pressure are determined by the distribution of all molecular species in the system, the potential of mean force effectively couples the position-dependent fluxes of the mobile species with the local density of all molecules: the mobile ions, solvent, and polyelectrolyte chains. As shown in this work, this coupling creates a link between the externally applied potential bias, the conformations of the polyelectrolyte in the channel, the local ionic concentrations and the ionic conductance of the nanopore.

We will assume that the fields  $\psi(\mathbf{r}, t)$  and  $\pi(\mathbf{r}, t)$  correspond to an extremum of  $W$ , and therefore the electrostatic potential instantaneously adapts to any change in the charge distribution of the system and the packing constraint is instantaneously fulfilled. The extremum of  $W$  with respect to  $\psi(\mathbf{r}, t)$  yields the Poisson equation

$$\varepsilon \nabla^2 \psi(\mathbf{r}, t) = -\langle \rho_Q(\mathbf{r}, t) \rangle \quad (10)$$

where  $\langle \rho_Q(\mathbf{r}) \rangle$  is the charge density at  $\mathbf{r}$  computed from the contribution of all charged species in the system. The extremum of  $W$  with respect to  $\pi(\mathbf{r}, t)$  yields the packing constraint, eq 6. It should be stressed that obtaining the Poisson equation for the relationship between the charge density and the electrostatic potential is a check of the consistency of the approach, since the Poisson equation always holds true.

The introduction of the packing constraint reduces the number of independent chemical potentials in the system by one. As a consequence, the chemical potentials in the theory are exchange chemical potentials.<sup>31</sup> In other words,  $\mu_i(\mathbf{r}, t)$  represents the work of placing a molecule of type  $i$  at  $\mathbf{r}$  while removing the equivalent volume of solvent molecules from the same position, see Supporting Information. Because the exchange chemical potential of the solvent is zero by definition, we have:

$$\frac{\delta \beta W}{\delta \rho_w(\mathbf{r}, t)} = \ln(\rho_w(\mathbf{r}, t)) + \beta \pi(\mathbf{r}, t) v_w = 0 \quad (11)$$

and from there it follows

$$\rho_w(\mathbf{r}, t) = \exp(-\beta \pi(\mathbf{r}, t) v_w) \quad (12)$$

This equation is the same as that obtained for the equilibrium case,<sup>31</sup> and it is a direct consequence of assuming that the packing constraint is instantaneously fulfilled.

At this point we introduce the steady-state condition. As a consequence, several simplifications to the general theory can be made. For instance, all variables are considered to be time-independent hereafter, and the following continuity equation is imposed:

$$\frac{\partial \rho_i(\mathbf{r})}{\partial t} = -\nabla \cdot \mathbf{J}_i(\mathbf{r}) = 0 \quad (13)$$

The polyelectrolyte chains are grafted to the pore walls, and therefore net mass fluxes of polymer cannot occur. Furthermore, in the steady state, the probability of each conformation is

time-independent, and thus the probability distribution of the polyelectrolyte conformations off-equilibrium will be the one that minimizes the functional  $W$  for the (fixed) density profiles  $\rho_i(\mathbf{r})$ , osmotic and electrostatic potentials that satisfy eqs 9–13. We thus get

$$P_P(\mathbf{r}', \alpha) = \frac{1}{\xi(\mathbf{r}')} \exp\left\{-\int n_P(\mathbf{r}', \alpha, \mathbf{r}) [f\beta\psi(\mathbf{r}) + v_P\beta\pi(\mathbf{r})] d\mathbf{r}\right\} \quad (14)$$

where  $n_P(\mathbf{r}', \alpha, \mathbf{r})d\mathbf{r}$  is the number of segments that a chain in conformation  $\alpha$  and grafted at  $\mathbf{r}'$  has in the volume element between  $\mathbf{r}$  and  $\mathbf{r}+d\mathbf{r}$ ,  $f$  is the charge of a monomer segment in units of elemental charge, and  $\xi(\mathbf{r}')$  is a normalization constant that ensures  $\sum_\alpha P(\alpha, \mathbf{r}') = 1$ .

In a general context, eq 14 assumes that the end-grafted polyelectrolyte can relax on the time scale of the experiment. This is always true in the steady state because the time scale of the experiment is assumed to be infinite. This condition is also fulfilled for processes slower than the polyelectrolyte conformational changes, such as protein adsorption.<sup>42</sup> If this approximation is not valid, kinetic equations for the polymer conformational changes should be given.

It is interesting to note that neglecting the osmotic pressure contribution in eq 9 results in the Nernst–Planck equation for the ions. The Nernst–Planck–Poisson approximation (the combination of the NP and the Poisson equations) has been widely used to describe ion conductivity in a variety of situations.<sup>1,10,57</sup> There are however important differences between our approach and NPP, in particular the fact that we explicitly include the size, shape, conformations, and charge distributions of all the molecular species. In other words, the differences between our theory and the NPP approach are (i) our framework can self-consistently treat the presence of grafted polyelectrolytes in the system, (ii) it includes excluded volume interactions between all the molecular species, and (iii) the coupling between the molecular organization, the charge distribution, and the different interactions leads to a nontrivial coupling between the electrostatic and osmotic fields that is completely absent in the NPP approach. In addition, as shown in previous work, the molecular theory can be easily generalized to consider the presence of chemical equilibria (acid–base,<sup>31</sup> redox,<sup>33</sup> ligand–receptor binding,<sup>50</sup> etc.), to include proteins in solution,<sup>50</sup> to study the kinetics and thermodynamics of protein adsorption,<sup>43</sup> and to consider van der Waals attractions between the different molecular species in the system.<sup>51</sup>

In order to solve the theory, we take advantage of the cylindrical symmetry of the system and assume that the densities, fields, and fluxes depend only on the  $r$  and  $z$  coordinates and are independent of the angular coordinate  $\theta$ ; namely, we solve the theory considering inhomogeneities in only two dimensions ( $r$  and  $z$ ). The required inputs are a large set of polymer conformations for each grafting point in the system, the salt concentration in the bulk, the applied potential ( $\Delta V$ ) and the molecular details of the polymer (segment volume and charge), the solvent molecules (molecular volume), and the ions (molecular volume, charge, and diffusion coefficient). For simplicity, we will assume that the diffusion coefficients  $D_i$  are those determined for the free ions in solution. This approximation is based on the high water content ( $\sim 85\%$ ) of the grafted polyelectrolyte layers modeled in this work. As outputs from the calculation, we get the distribution of the ions and polymer in the system, the electrostatic potential

at each position, and the position-dependent ion fluxes. The total current through the system,  $I$ , can be then determined from the integration of the axial component of the total ionic fluxes in the plane normal to the axis passing through  $z = 0$ . The reader is referred to the Supporting Information for more detailed explanations of the formulation, derivation, and solving procedure of the theory, including how the polymer chain conformations are generated.

### 3. RESULTS AND DISCUSSION

#### 3.1. Low Bias Molecular Organization and Conductance.

We start our discussion by considering the case where the applied bias is very small. In this regime, the distributions of the mobile species in the system and the conformations of the polymers are very close to those in equilibrium. In Figure 2A we show color maps for the polymer volume fraction and current flux lines for three different scenarios: the bare pore, a pore with chains grafted only on the inner walls (system I), and a pore with chains grafted both on the inner and outer walls (system II). For system I, the figure shows that even though chains are grafted only inside the pore, there is a finite density of segments in the reservoirs. This occurs because polymer chains tend to stretch out from the pore in order to minimize the electrostatic repulsions and the osmotic pressure and to maximize their conformational entropy.<sup>47</sup> For system II, the brush layer inside the pore shows a density of polymer segments higher than that on the outer walls (even though the grafting density is the same in both cases). This effect is another manifestation of the confined environment inside the pore.

Figure 2A also shows the current flux lines and vectors for the different systems under analysis. The current flux lines are tangential to the current flux vectors at each point. The current flux vectors indicate the direction and magnitude of the total ionic current flux,  $-\sum_{i=A,C} |e| q_i J_i(r, z)$  (where  $|e|$  is the unit of elemental charge), at each position. The current flux lines calculated for the bare pore/reservoirs system run parallel to the axis inside the pore, and their magnitude is constant along the  $r$  coordinate. In the reservoirs they adopt a hemispherical symmetry (for example, for the upper reservoir they run normal to the hemispherical surfaces with an origin at  $r = 0$  and  $z = L/2$ ). The size of the blue arrows shows that current fluxes are much more intense inside the pore than in the reservoirs (note that the blue arrows far away from the pore are too small to be seen). This is because the total ionic current flows through a cross-section area of  $\pi R^2$  inside the channel but through a larger area of  $2\pi r^2$  for a hemispherical shell of radius  $r$  ( $r > R$ ) in the reservoirs.

For system I, current flux lines inside the pore are affected by the presence of the grafted polyelectrolyte. Namely, current fluxes are higher in the regions of the pore with high polyelectrolyte density. In order to explain this observation, let us turn to our previous work on the pH-dependent conductance of long nanochannels.<sup>32</sup> We have shown there that the predicted conductance is governed by the incorporation of counterions inside the channel that is required to compensate the charge of the grafted polyelectrolytes. This local increase in the number of charge carriers produces an increase in the conductance of the polyelectrolyte-modified channel with respect to the unmodified one. This result was found to quantitatively agree with the increase in conductivity observed for a long nanochannel modified by protonated poly(vinyl pyridine) with respect to the bare one.<sup>9,32</sup> It is also in qualitative agreement with experiments in

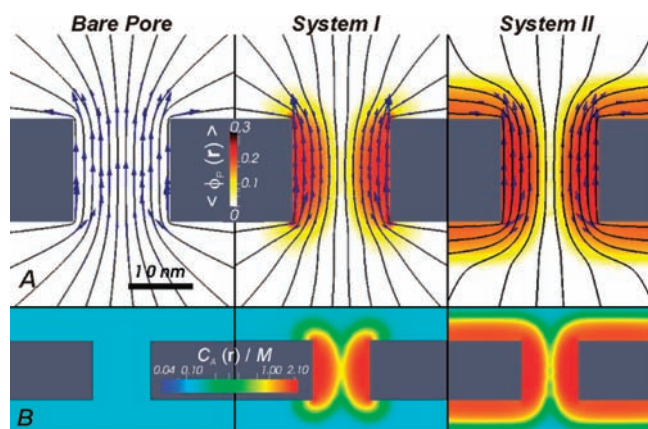


**Figure 2.** A. Polymer volume fraction color maps for a cut along a plane containing the pore axis for a bare pore, system I (chains tethered inside the pore) and system II (chains tethered inside and outside the pore) under a low applied bias ( $\Delta V = +10$  mV) for a positively charged polyelectrolyte (charge per monomer,  $f = 0.5$ ). Blue arrows show the direction and magnitude of the current flux vectors, and black lines are the flow lines for this vector field. For better visualization, different scales have been used for the current flux vectors in different panels: an arrow of length 1 nm represents  $1.3 \times 10^{-13}$  A·nm<sup>-2</sup> for the bare pore,  $3.3 \times 10^{-13}$  A·nm<sup>-2</sup> for system I, and  $5.0 \times 10^{-13}$  A·nm<sup>-2</sup> for system II. B. Molar anion concentration color maps for the systems in A (note that a logarithmic scale has been used). Calculation parameters: chain length,  $N = 20$ ; surface coverage,  $\rho_G = 0.5$  nm<sup>-2</sup>; pore radius,  $R = 7.5$  nm; pore length,  $L = 16$  nm; bulk salt concentration,  $C_{\text{salt}} = 0.1$  M. For system II chains are grafted to the outer wall up to  $R_p = 39.5$  nm.

biconical nanopores asymmetrically modified with poly(acrylic acid) brushes that display an ‘open state’ conductance (i.e., for basic pH and negatively applied voltages) that is larger than that measured before the grafting process.<sup>12</sup> The same mechanism described for long channels is predicted to operate in the nanopore. Figure 2B shows that, in fact, the anion concentration for short nanopores follows the distribution of the positively charged polymer segment density and can be as high as 2 M (i.e., 20 times larger than the bulk solution ionic strength of 0.1 M) in polyelectrolyte rich regions. While the concentration of counterions is predicted to be enhanced by a factor of 20 inside the polymer brush with respect to that in the bulk solution, the concentration of co-ions (cations) in the polyelectrolyte-rich regions drops almost by the same factor (note however that the total concentration of charge carriers inside the pore, anions plus cations, is enhanced).

The current flux lines inside the pore for system II behave in the same way as those for system I. On the other hand, the current fluxes in the reservoir for system II are enhanced close to walls due to the presence of the polyelectrolyte brush. Far away from the surface of the membrane, the current flux lines in the reservoir retain their hemispherical symmetry.

In Figure 3 we show the total conductance of the pore,  $G$  ( $G = 1/\Omega$ , where  $\Omega$  is the pore resistance) as a function of its length for the different systems described above and two different (experimentally relevant) grafted polymer surface coverages. The effect of increasing the surface coverage for pores of any length for the systems shown in Figure 3 is to produce a higher local counterion concentration and thus an increase in the conductance of the system. All curves present two well-defined regimes.<sup>52</sup> For  $L \ll R$ , the conductance is independent of  $L$

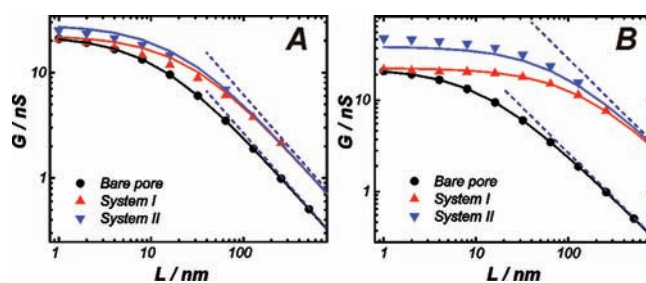


**Figure 3.** Low bias ( $\Delta V = 10$  mV) conductance for the bare pore, system I and system II as a function of pore length, and two different surface coverages (for system I and II):  $0.1 \text{ nm}^{-2}$  (A) and  $0.5 \text{ nm}^{-2}$  (B). Symbols and solid lines show the predictions of the steady-state molecular theory and the simple conductance model, respectively. Dashed blue lines show the predictions of the molecular theory using the GCF approximation for the conductance calculation as described in ref 32 (valid for long pores). Calculation parameters: chain length,  $N = 20$ ; charge per monomer,  $f = 0.5$ ; pore radius,  $R = 7.5$  nm; bulk salt concentration,  $C_{\text{salt}} = 0.1$  M. For system II chains are grafted to the outer wall up to  $R_p = 39.5$  nm.

because the electrical resistance of the whole system is dominated by that of the reservoirs. In this regime, the conductances predicted for system I and for the bare pore/reservoirs system converge to the same value as  $L$  decreases because the reservoirs are identical in both systems. On the other hand, the conductance of system II for  $L \ll R$  is higher than that of system I because the polyelectrolyte chains grafted to the outer walls enhance the counterion concentration close to the membrane with the subsequent decrease in the access resistance. It is noteworthy that grafting chains to the outer walls can increase the low bias conductance of the system by a factor of  $\sim 2$  for short nanopores. In other words, any increase in conductance observed for very short pores upon grafting a polyelectrolyte layer would probably result from the modification of the outer surface rather than from the modification of the pore itself.

For  $L \gg R$ , the conductance decreases as  $L$  because the total resistance is dominated by that of the solution inside the pore. In this regime the conductance is sensitive to the inner chemistry of the pore but not to the chemistry of the outer walls: the predictions for system I and II converge to a value higher than that for the bare pore. Under these conditions, the conductance of the system can be well described within the GCF approximation<sup>53</sup> (dashed lines in Figure 3). It is interesting to note that the formulation of the nonequilibrium molecular theory presented in this work is very well suited to model short nanopores ( $L < 1 \mu\text{m}$ ), but the calculations become prohibitively expensive for very long channels. On the other hand, the combination of GCF approximation and the molecular theory presented in ref 32 is valid for long nanochannels ( $L > 1 \mu\text{m}$ ), but the approximation breaks down for short pores. Both approaches are therefore complementary and are based on the same free energy formalism.

The factor controlling the local conductance for the systems in Figures 2 and 3 is the local enhancement in the counterion concentration due to the grafted polyelectrolytes, which is reasonable for highly charged polyelectrolytes. The effect of neutral end-grafted polymers (or even weakly charged polyelectrolytes) on ionic conductance is completely different, as shown next. In a pore modified with a neutral polymer, the current fluxes close to the pore inner walls are smaller than those close to pore axis (Figure 4A) because the concentration of both

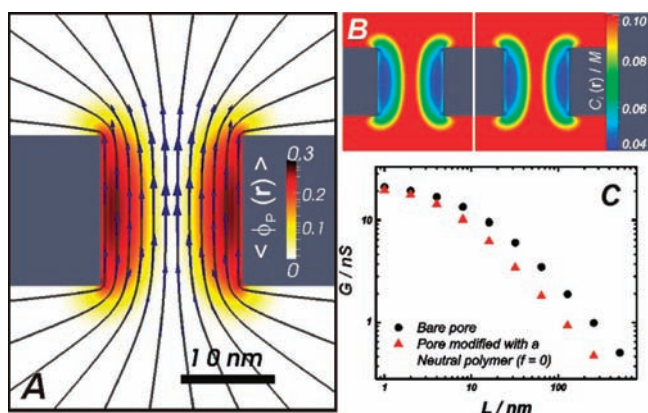


**Figure 4.** A. Polymer volume fraction color maps for a cut along a plane containing the pore axis for a pore modified with neutral ( $f=0$ ) chains (grafted only inside the pore) under a low bias ( $\Delta V = 10$  mV). An arrow of 1 nm indicates a current flux vector of  $1.3 \cdot 10^{-13}$  A $\cdot$ nm $^{-2}$ . B. Molar anion (left) and cation (right) ion concentration color maps for the system shown in A. C. Low bias ( $\Delta V = +10$  mV) conductance for the bare pore and a pore with neutral polymers as a function of the pore length. Calculation parameters: chain length,  $N = 20$ ; pore radius,  $R = 7.5$  nm; pore length,  $L = 16$  nm (for panels A and B); bulk salt concentration,  $C_{\text{salt}} = 0.1$  M.

negative and positive ions in the polymer-rich region is depleted (Figure 4B). This drop in local ion concentration inside the pore is the same for cations and anions and can be traced back to excluded volume interactions. As a result of the decrease of the number of charge carriers in the pore, the conductance of the polymer-modified pore is smaller than that of a bare pore (Figure 4C). This result is in agreement with recent experimental results where a drop in conductance was observed upon grafting weakly charged proteins into a single short pore.<sup>54</sup> We also observe that the drop in conductance is larger in long channels than in short nanopores because in the latter the total resistance is dominated by that of the reservoirs.

Because salt ions in solution screen the Coulombic forces in the system, it is interesting to analyze how the ionic strength affects the balance between electrostatic and excluded volume interactions. As shown above, the conductance for system I in Figure 3 (0.1 M bulk ionic strength) is enhanced with respect to the bare pore due to counterion uptake by the brush. In that case, the low potential bias conductance for the polyelectrolyte-modified pore is 20 nS in comparison with 9.5 nS for the bare pore. However, in a 1.0 M electrolyte solution the excluded volume interactions become dominant and the conductance of the polyelectrolyte-modified pore (82 nS) is slightly smaller than that predicted for the bare one under the same conditions (95 nS).

While the molecular theory provides detailed predictions on the organization and ionic conductance of the nanopore, simplified analytical models are useful for routine analysis of experimental data and for understanding the physical mechanisms that govern the behavior of the system. We present here a simplified model (derived and described in detail in the Supporting Information) in which the system resistance is approximated as the in series combination of the pore and reservoirs (access) resistances. For each reservoir, the access resistance is further subdivided into two contributions: (i) the resistance from the bulk up to  $r = R$  (border of the pore) and (ii) the resistance of the hemisphere located at the mouth of the pore (the hemisphere of

radius  $R$  centered at  $r = 0$  and  $z = -L/2$  or  $L/2$ ). The first contribution accounts for both the conductance through the bulk solution and (for system II) through the brush grafted to the outer walls. The resistance according to the simplified model is given by

$$\Omega = \frac{1}{\pi\sigma_s} \left[ \frac{\sigma_s}{h_w\sigma_w} \left( \ln \left( R + \frac{h_w\sigma_w}{\sigma_s} \right) - \ln(R) \right) \right] + \frac{1}{\pi} \frac{L}{h_i(2R - h_i)\sigma_i + (R - h_i)^2\sigma_s} + \left( \frac{1}{2} - \frac{1}{\pi} \right) \frac{1}{\sigma_s R} \quad (15)$$

where the terms on the right-hand side represent the reservoir resistance from infinity up to the edge of the pore, the resistance of the pore itself, and the resistance of the hemisphere located at the mouth of the pore, respectively. In eq 15,  $\sigma_s$  is the conductance of the bulk solution which is estimated from the bulk salt concentration and ion mobilities,  $\sigma_i$  and  $h_i$  are the conductance of the solution confined inside the brush layer grafted to the pore inner walls and the thickness of this layer, respectively, and  $\sigma_w$  and  $h_w$  are the conductance of the solution confined in the brush grafted to the outer walls and the thickness of the brush, respectively. Equation 15 can be further simplified for the different cases under study. The parameters of eq 15 can be estimated using Donnan partition arguments<sup>55,56</sup> from the polyelectrolyte surface coverage, the number of segments per chain, and the charge per segment as explained in the Supporting Information. The resulting expressions are:

$$\Omega = \frac{1}{\pi\sigma_s} \left[ \frac{2C_{\text{salt}}}{f\rho_G N} \left( \ln \left( R + \frac{1}{2} \frac{f\rho_G N}{C_{\text{salt}}} \right) - \ln(R) \right) \right] + \frac{1}{\pi} \frac{C_{\text{salt}} L}{fN\rho_G R\sigma_s} + \left( \frac{1}{2} - \frac{1}{\pi} \right) \frac{1}{\sigma_s R} \quad (16)$$

for system II;

$$\Omega = \frac{1}{2R\sigma_s} + \frac{1}{\pi} \frac{C_{\text{salt}} L}{fN\rho_G R\sigma_s} \quad (17)$$

for system I and

$$\Omega = \frac{1}{2R\sigma_s} + \frac{1}{\pi\sigma_s} \frac{L}{R^2} \quad (18)$$

for the bare pore.

The conductance ( $G = 1/\Omega$ ) predicted by these equations is shown (solid lines in Figure 3) to be in good agreement with the prediction of the full nonequilibrium molecular theory. It is worthwhile to note that this comparison requires no fitting parameters. Furthermore, for the bare pore/reservoirs system, the conductance can be expressed as a function of a single universal variable,  $L/R$  (the aspect ratio). In the Supporting Information we show that the prediction of nonequilibrium theory and the simple model for this system are in very good agreement for several combinations of  $R$  and  $L$ . The small discrepancies between the molecular theory and the simple analytical model observed in Figures 3, and Figure 3S in Supporting Information, for very short pores (both bare or polyelectrolyte modified) may have an origin in the approximations made to calculate the resistance at the mouth of the pore.

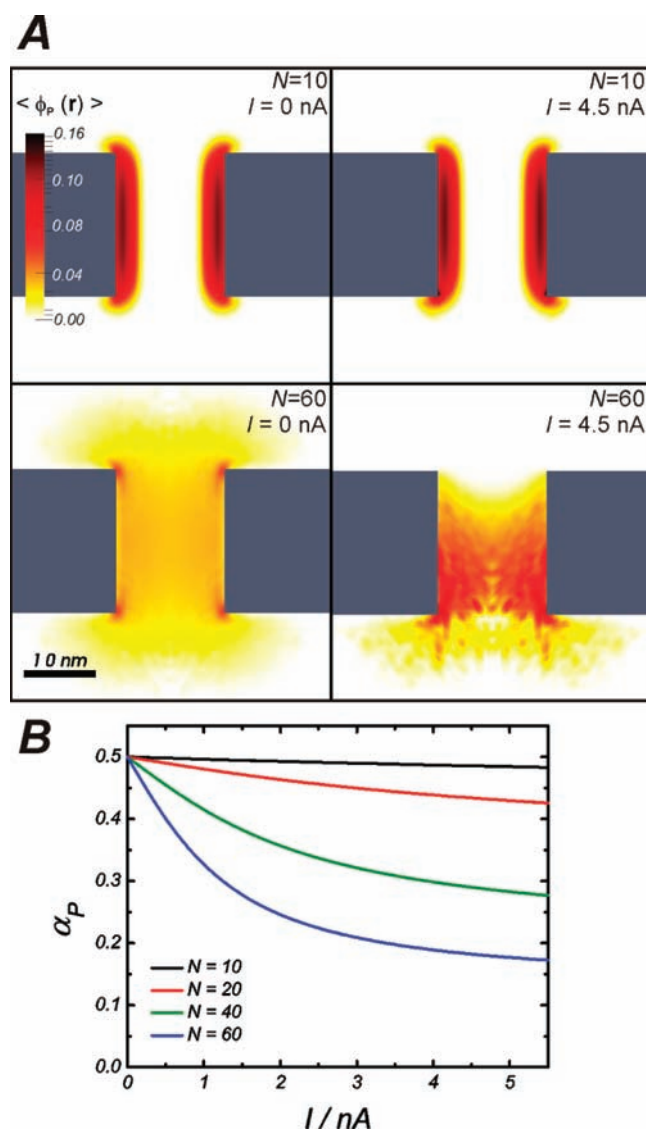


**Figure 5.** A. Polymer volume fraction color maps for a cut along a plane containing the pore axis for system I (chains tethered inside the pore) for  $N = 10$ ,  $\rho_G = 0.3$  chains  $\cdot$  nm $^{-2}$  (upper panels) and  $N = 60$ ,  $\rho_G = 0.05$  chains  $\cdot$  nm $^{-2}$  (lower panels). Plots are shown for  $I = 0$  ( $\Delta V = 0$ , right panels) and  $I = 4.5$  nA ( $\Delta V = 0.5$  V for  $N = 10$  and  $\Delta V = 0.28$  V for  $N = 60$ , left panels). Other calculation parameters: pore radius,  $R = 7.5$  nm; pore length,  $L = 20$  nm; bulk salt concentration,  $C_{\text{salt}} = 0.1$  M. The same color scale has been used for all plots. B. Plot of the excess of segments at  $z > 0$  (upper half of the pore) as defined in eq 19 as a function of the total ionic current through the system.

We should finally briefly comment on the range of application of eqs 16–18. These equations have been derived to describe nonregulating polyelectrolytes and thus are valid only for strong polyelectrolytes or for weak polyelectrolytes in solutions of pH very far from the monomer  $pK_a$  ( $\text{pH} \gg pK_a$  for polyacids or  $\text{pH} \ll pK_a$  for polybases). Further, they are valid only for low applied potentials, because (as shown in the next section) ion and polyelectrolyte reorganization occurs at high  $\Delta V$ .

**3.2. Large Applied Bias Molecular Organization and Ionic Conductance.** For large applied potential bias, the distribution of ions and polyelectrolyte in the system can dramatically differ from that in equilibrium. In Figure 5A we show the predicted

polymer volume fraction color maps for a short pore with polyelectrolytes grafted only at the inner walls (system I) in equilibrium ( $\Delta V = 0$ ,  $I = 0$ ) and in the steady state for an applied potential that gives a current  $I = 4.5$  nA. The dimensions of the pore ( $L = 20$  nm and  $R = 7.5$  nm) correspond to the typical dimensions of pores drilled in SiN membranes.<sup>57</sup> The two systems shown in Figure 5A present both different chain lengths ( $N = 10$  and  $N = 60$ ) and surface coverages ( $\rho_G = 0.3$  and  $0.05$  chains  $\cdot$  nm $^{-2}$ , respectively). These parameters were chosen in order to keep constant the product  $N\rho_G$  because this product controls the contribution of the pore to the total conductance of the pore/reservoirs system in the low applied bias limit (see eqs 16 and 17). In other words, we will compare pores with the same total number of polymer segments but different chain lengths and surface densities. Note also that we compare systems with the same total ionic current instead of the same applied potential because the former parameter is more relevant for the ionic concentration polarization effects,<sup>58–60</sup> see below. The plots in Figure 5A show that the positively charged polyelectrolytes are repelled from the positively biased reservoir and that the magnitude of the effect dramatically depends on chain length. It is important to note that the deformation of the polymer layer due to the applied bias is a consequence of the ionic currents flowing through the system, which determine the electrostatic potential felt by the polyelectrolyte chains. These forces can be measured, as was demonstrated for DNA chains in solid-state nanopores.<sup>61</sup> Moreover, electromechanical manipulation of polyelectrolytes in nanopores has been proposed as a method to gate ionic currents.<sup>62</sup> As an example, the insertion/expulsion of DNA layers grafted inside conical nanopores driven by applied bias was proposed to block/unblock the mouth of the pore, creating a rectifying behavior.<sup>22,63</sup> Ionic rectification due to electromechanical gating has been proposed also for trapped DNA threads in biological nanopores.<sup>64</sup>

The effect of chain length on the degree of polyelectrolyte deformation can be understood in terms of the fraction of segments located at the upper half of the pore (with respect to the total number of polymer segments in the system) as a function of the total current passing through the system. This fraction is defined as:

$$\alpha_p = \frac{\int_0^\infty dz \int_0^\infty r dr \langle \phi_p(r, z) \rangle}{\int_{-\infty}^\infty dz \int_0^\infty r dr \langle \phi_p(r, z) \rangle} \quad (19)$$

where  $\langle \phi_p(r, z) \rangle$  is the volume fraction of polyelectrolyte segments at  $r$  and  $z$ . The limiting values of  $\alpha_p$  are 0 (all segments at  $z < 0$ ) and 1 (all the segments at  $z > 0$ ). In equilibrium, the system is symmetric and thus,  $\alpha_p = 0.5$ . Figure 5B shows a plot of  $\alpha_p$  vs the total ionic current ( $I$ ) for the systems in Figure 5A and two additional systems with different chain lengths (but with the same  $N\rho_G$ ). Applying a positive bias to the upper reservoir causes the positively charged chains to stretch toward the lower reservoir and thus  $\alpha_p < 0.5$  for all  $\Delta V > 0$ . The degree of deformation increases with the chain length as a consequence of the increase in polymer flexibility.

The distribution of the polymer volume fraction inside the pore is regulated by the competition between the length of the chain and the length of the pore. For example, in Figure 6A we compare the system of  $N = 60$  for  $I = 0$  and 2 nA and two different pore lengths: 20 and 128 nm. The reorganization in the short

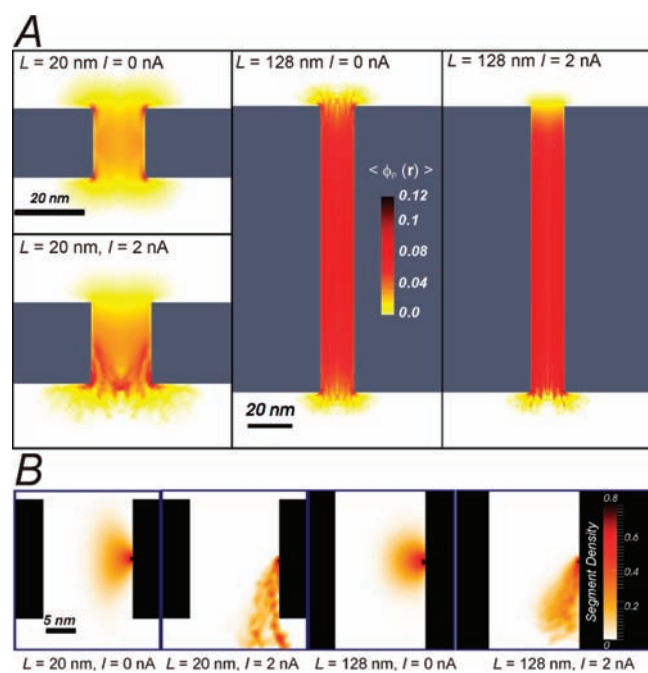


**Figure 6.** A. Polymer volume fraction color maps for a cut along a plane containing the pore axis for system I (chains tethered inside the pore) for  $N = 60$ ,  $\rho_G = 0.05$  chains  $\cdot$  nm $^{-2}$  and  $L = 20$  nm or  $L = 128$  nm. Plots are shown for  $I = 0$  ( $\Delta V = 0$ ) and  $I = 2.0$  nA ( $\Delta V = 0.15$  V for  $L = 20$  nm and  $\Delta V = 0.4$  V for  $L = 128$  nm). The same calculation parameters of Figure 5 were used. B. Single chain segment density projections on the  $x,z$  plane for the systems in A. The chain shown is grafted at  $y = 0$ ,  $x = R$  and  $z = 0$ .

pore is more dramatic than in the long one, which is supported by the values of  $\alpha_p$  of 0.24 and 0.45 for  $L = 20$  and 128 nm, respectively (for an infinitely long pore, the value of  $\alpha_p$  should approach 0.5). For the long pore, the effect of the applied potential on the polyelectrolyte density is only apparent at pore entrances. However, this observation does not imply that the conformations of the chains inside the long pore are insensitive to the applied bias. For instance, the single chain density plots for a polyelectrolyte end-grafted in the middle of the pore ( $z_{\text{graft}} = 0$ ) shown in Figure 6B indicate that chain deformation for  $I = 2$  nA occurs both for the long and short pores. Inside the long pore the optimal polymer densities in equilibrium and under an applied bias are the same, although the molecular organizations of the chains giving rise to these density profiles are different. Single chain profiles in equilibrium ( $I = 0$  nA) show an elongation in the axial direction for the chains in the short pore. This effect is caused by the presence of the reservoirs as discussed in a previous publication.<sup>47</sup>

We have chosen to compare systems with the same current in Figure 6, and thus the applied bias for the short pore (0.15 V) is smaller than that for the long one (0.40 V). Comparing systems at constant potential will yield much lower currents for long nanochannels in comparison with short pores and therefore less polymer deformation. For very long nanochannels under moderate applied potential biases, polymer deformation will not occur and the equilibrium structure determines the conductance of the pore (GCF approximation).<sup>32</sup>

Figure 7 shows the electrostatic potential for the systems in Figure 5A. It is clear that the electrostatic potential has contributions from both charges on the polyelectrolyte and the externally applied bias (see plots for  $N = 10$ ). However, it is worthwhile to point out

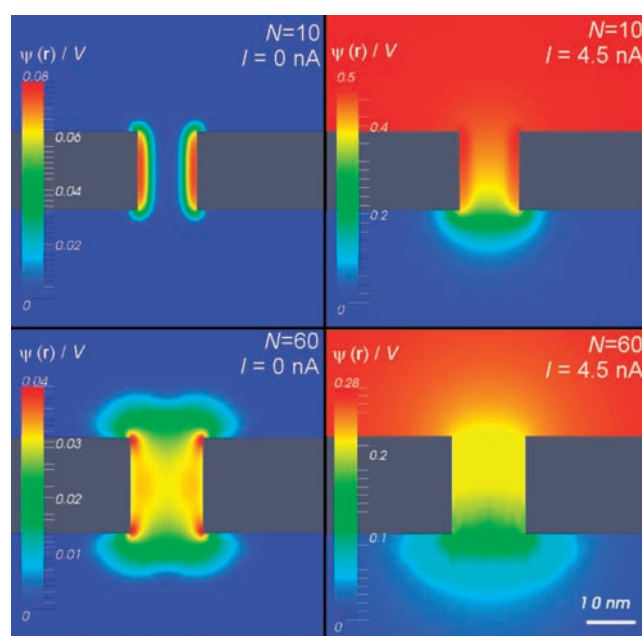


**Figure 7.** Electrostatic potential color maps for the systems shown in Figure 5A.

that the electrostatic potential is not the sum of the externally applied bias and the field created by the polyelectrolyte in equilibrium because, as we have shown above, there is a redistribution of the polyelectrolyte and ions due to the applied electrostatic potential.

Since the conductance is determined by ion distribution, it is insightful to analyze how the concentration of the majority carriers (anions) evolves as a function of the applied bias. Figure 8 shows color maps of the concentration of anions for the systems in Figure 5A and 7. We note that the anion concentration in the steady state presents a depletion region close to the pore entrance in the lower reservoir and an enhancement region at the mouth of the upper one. This effect is known as concentration polarization and arises due to the presence of charges on the inner pore surface.<sup>58–60,65</sup> Briefly, the concentration polarization regions develop when the mass diffusion of the majority carrier from the bulk to the pore entrance cannot sustain the current through the pore. Therefore, in the lower reservoir the concentration near the pore entrance decreases in order to create a concentration gradient to drive the diffusion flux from the bulk into the pore. Following the same explanation, a concentration gradient also is developed in the upper reservoir (and therefore an enhancement region shows up) in order to increase the flux of anions from pore mouth to the upper bulk solution. The concentration of the minority carrier (cations not shown) follows a similar distribution to that of the majority carrier because separating ionic charges beyond a few nanometers in aqueous solution implies a very high energy cost (note however that our theory does not impose local electroneutrality).

The concentration profiles along the pore axis (plotted in Figure 8B) show that upon applying the potential bias there is an increase in the total anion concentration inside the pore for the two chain lengths under study, similar to that described for a pore bearing a surface charge in ref 58. The profiles also show the concentration polarization depletion region that develops just on the pore entrance. This mechanism is supported by the plots of the excess of anions and cations in the upper half of the system



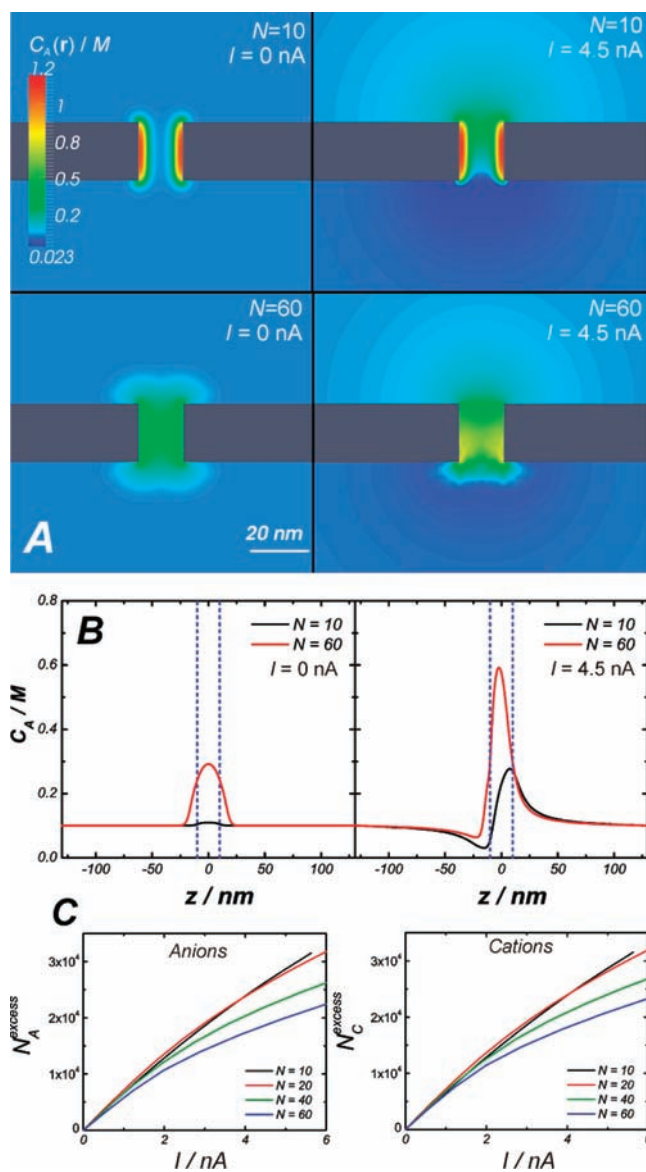


**Figure 8.** A. Anion molar concentration color maps for the systems shown in Figure 5A. B. Concentration profiles along the pore axis ( $r = 0$ ) for the systems shown in A. Dotted blue lines show the position of the membrane surfaces. C. Plot of the number excess of anions and cations at  $z > 0$  (upper half of the pore) as defined in eq 20 as a function of the total current through the pore.

with respect to the lower half as a function of the total current (Figure 8C). The latter quantity is defined as:

$$N_i^{\text{excess}} = 2\pi \left[ \int_0^\infty dz \int_0^\infty r dr C_i(r, z) - \int_{-\infty}^0 dz \int_0^\infty r dr C_i(r, z) \right] N_A \quad (20)$$

where  $C_i(r, z)$  is the molar concentration at  $r$  and  $z$  and  $N_A$  is Avogadro's number. Figure 8C shows that both the concentration of anions and cations is depleted in the lower half (i.e., there is an excess of ions in the upper half,  $N_i^{\text{excess}} > 0$ ).

An interesting observation is that the concentration polarization depletion region in Figure 8A and 8B for the system with  $N = 60$  is smaller than that for  $N = 10$  (for the same total current). This observation is supported by the smaller value of  $N_i^{\text{excess}}$  for

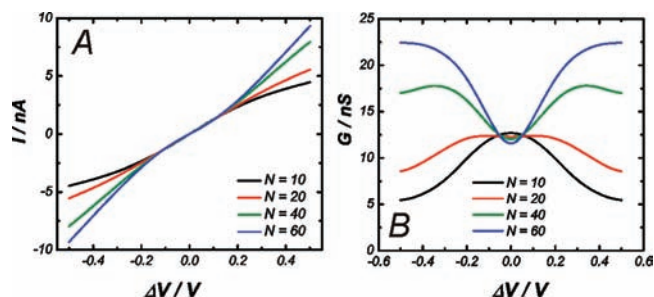


**Figure 9.** A. Current–potential curves predicted by the steady-state molecular theory for system I (chains tethered only inside the pore) for different chain lengths and surface coverages but conserving the total number of segments (constant  $N\rho_G$ ). B. Differential conductance  $G = \partial I / \partial \Delta V$  vs  $\Delta V$  for the systems in A. Same calculation parameters as in Figure 5.

$N = 60$  compared with  $N = 10$  for a given total current in Figure 8C. This dependence on chain length can be traced back to the polyelectrolyte distribution shown in Figure 5A. In the system with  $N = 60$ , the polyelectrolyte layer readily deforms with the applied bias, creating a region with a high density of positively charged segments at the lower entrance of the pore. The presence of these segments in the lower reservoir decreases the magnitude of the anion depletion process compared with a system where almost no segment redistribution occurs due to the applied potential ( $N = 10$ ).

The complexity of the molecular organization in the steady state, described in the previous paragraphs, arises from the coupling between ion concentration and fluxes, the conformation of the polyelectrolyte chains and the electrostatic potential. The question is how this organization impacts the experimentally accessible current–potential curves. Figure 9A shows that the  $I$  vs  $\Delta V$  curves for the different chain lengths under study present a linear (i.e., ohmic) response in a region close to the origin. This is in fact the region discussed in the previous section (low bias molecular organization and conductance), in which the redistribution of the polyelectrolyte and ions has a minor effect on the  $I$  vs  $\Delta V$  curves and thus the simplified model given by eqs 16–18 is valid. When the absolute value of applied potential is increased beyond this ohmic regime, positive deviations to linearity appear for long chains, while negative deviations show up for short chains (Figure 9B). The drop in conductance with  $\Delta V$  for short chains is expected due to the concentration polarization effect. Moreover, a limiting constant current is expected for applied potentials larger than those studied in this work.<sup>58–60</sup> On the other hand, the increase in conductance with  $\Delta V$  exhibited by longer chains is unexpected. As shown above, increasing the applied bias deforms the polyelectrolyte layer for long chains, resulting in a redistribution of the positive polyelectrolyte segments to the lower mouth of the pore. This process leads to a decrease in resistance with the applied potential because (i) it inhibits the formation of the anion depletion layer (as shown in Figure 8) and it reduces the concentration polarization effect, therefore enhancing the conductance. This mechanism is supported by the fact that very long channels (for which the pore resistance is always larger than the access resistance) exhibit ohmic and chain-length independent conductance in the potential range of Figure 9 (see Figure 4S, Supporting Information), (ii) it decreases the concentration of positively charged segments inside the pore, increasing the concentration and flux of the

co-ions (cations). For example, the fraction of current carried by the majority carrier (anions) for  $I = 1.0$  nA (linear regime) is 0.89 for  $N = 10$  and 0.86 for  $N = 60$ ; on the other hand, for  $I = 4.5$  nA (nonohmic regime) this fraction becomes 0.85 for  $N = 10$  and 0.76 for  $N = 60$ . (iii) The expulsion of polyelectrolyte segments from the pore also decreases the excluded volume interactions with both ions. The coupled nature of the problem makes it impossible to separate the contributions from each mechanism, although it is clear that the increase in conductance with the applied bias arises from the reorganization of the long polyelectrolyte chains. For instance, a neutral grafted brush (that interacts through excluded-volume interactions only) does not deform with the applied bias and thus leads to ohmic conductance (Figure 5S, Supporting Information). The decrease in resistance with the applied bias predicted for long deformable polyelectrolyte chains creates an experimentally accessible fingerprint for their presence inside the nanopore.

#### 4. CONCLUSIONS

In the present work, a nonequilibrium molecular theory was introduced to study ion conductance in cylindrical nanopores and nanochannels modified with supramolecular structures. Molecular theories are required to study these systems because the molecular details are important, but the length and time scales involved make them formidable problems to attack with computer simulations. The short nanopores systems analyzed in this work require a nonequilibrium description of the pore/reservoir system involving inhomogeneities along at least two coordinates. This is in contrast to long channels that can be treated within the Goldman Constant Field (GCF) approximation because the resistance at pore ends can be neglected. In that case, the channel conductance can be determined from the equilibrium concentration of charge carriers (ions) inside the channel, and the symmetry of the system allows the consideration of only inhomogeneities in the radial coordinate.<sup>32,53,58</sup>

We have shown that the molecular organization of the pore/reservoir system arises from the interplay between ion fluxes and concentration, polyelectrolyte organization, and electrostatic and nonelectrostatic interactions. Grafting polyelectrolyte chains inside a nanochannel enhances its conductance due to the local increase in counterion concentration required to balance the charges on the polyelectrolyte. However, this effect is of minor importance for very short pores where the total resistance is dominated by that of the reservoirs. In such cases, any increase in conductance upon grafting polyelectrolyte chains should be due to the modification of pore outer walls. Along the same lines, grafting a neutral polymer inside a nanopore decreases its conductance, and the magnitude of the effect is larger for longer pores. These results suggest that long channels are more suitable for sensor applications than nanopores.

For a large applied bias, the organization of the system becomes very complex and gives rise to unexpected behavior of the conductance. For example, in the low applied bias regime the conductance of the pore depends on the total number of polyelectrolyte segments (Figure 9). In other words, it depends on the product of chain length and surface coverage but not on the individual values of these parameters. However, this behavior is no longer valid in the large applied potential regime because longer chains at low grafting density are more readily to deform than short chains at high surface coverage. The deformation of long chains gives rise to an unexpected behavior, the decrease of

system resistance with the applied bias shown in Figure 9B. This exemplifies how our intuition and the current theoretical tools developed for bare nanopores may fail to describe the behavior of nanopores modified by supramolecular structures if the coupling between ion fluxes and the conformational degrees of freedom of the polyelectrolytes are not taken into account.

One limitation of the present approach is that it neglects transport of momentum in the system and therefore any electroosmotic effects. This contribution to the overall current has been shown to be of secondary importance in previous solutions of the NPP and Navier–Stokes equations for surface-charged nanochannels and nanopores.<sup>58</sup> In the case of polyelectrolyte-modified nanopores, the presence of the grafted polyelectrolyte can hinder the solvent fluxes through the pore and (as discussed in Appendix C of ref 52, where off-diagonal Onsager couplings between charge and mass fluxes are taken into account) blocking the solvent fluxes will prevent the electroosmotic contributions to the total current. Thus, we do not expect that the results presented in this work will be qualitatively affected by electroosmotic effects. However, these effects are essential to describe other interesting phenomena such as mechanical to electric energy conversion in nanochannels.<sup>23,24</sup> Moreover, the behavior of polymer brushes under solvent flow is an active research area.<sup>66,67</sup> For these reasons, their inclusion in our theoretical framework remains an important research direction.

The theory presented in this work is based on a mean-field description of the molecular species in the system, while the mass fluxes are described within a linear response approximation. The range of validity of these combined approximations is difficult to assess. We are however confident about the predictions of the theory for the present system based on our previous work for long nanopores that had shown very good agreement between theoretical predictions and experimental observations<sup>32</sup> and previous work on a simpler system that has shown good agreement between simulations and linear response—mean field theories.<sup>39</sup> We expect that new developments in solid-state nanopores and macromolecular synthesis will provide systematic measurements on well-characterized systems, which can be used to test theoretical models. In this direction, further work is necessary to expand our model abilities in order to address the role of the complex geometries usually found in experiments, such as hourglass,<sup>54,68,69</sup> conical,<sup>10,11,15,16,18,20,22</sup> and biconical pores.<sup>12,14,17,19</sup> Incorporation of chemical equilibrium and additional nonelectrostatic interactions (i.e., hydrophobic interactions) is also of interest for the description of experimental studies involving weak and/or hydrophobic polyelectrolytes. To conclude, we expect that as the widespread interest in chemically modified nanopores and nanochannels continues growing, molecular theories will be developed to model their equilibrium and dynamical properties and thus to play a central role in their analysis, understanding, and design.

#### ■ ASSOCIATED CONTENT

Supporting Information. Detailed description of the molecular theory and numerical methods, simple model for ion conduction in nanopores, comparison between the predictions of the simple model and the molecular theory for neutral pores, and  $I$  vs  $\Delta V$  curves for long pores ( $L = 256$  nm). This material is available free of charge via the Internet at <http://pubs.acs.org>.

## AUTHOR INFORMATION

## Corresponding Author

igalsz@northwestern.edu

## ACKNOWLEDGMENT

This material is based upon work supported as part of the NERC (Non-Equilibrium Research Center), an Energy Frontier Research Center funded by the U.S. Department of Energy, Office of Science, Office of Basic Energy Sciences under Award Number DE-SC0000989. Y.R. would like to acknowledge the support by grants from the Israel Science Foundation and from the US-Israel Binational Science Foundation.

## REFERENCES

- (1) Daiguji, H. *Chem. Soc. Rev.* **2010**, 39, 901.
- (2) Dekker, C. *Nat. Nanotechnol.* **2007**, 2, 209.
- (3) Wang, G.; Zhang, B.; Wayment, J. R.; Harris, J. M.; White, H. S. *J. Am. Chem. Soc.* **2006**, 128, 7679.
- (4) Plecis, A.; Schoch, R. B.; Renaud, P. *Nano Lett.* **2005**, 5, 1147.
- (5) Stein, D.; Kruithof, M.; Dekker, C. *Phys. Rev. Lett.* **2004**, 93, 035901.
- (6) Hou, X.; Jiang, L. *ACS Nano* **2009**, 3, 3339.
- (7) Adiga, S. P.; Brenner, D. W. *Nano Lett.* **2005**, 5, 2509.
- (8) Cheng, L. S.; Cao, D. P. *ACS Nano* **2011**, 5, 1102.
- (9) Yameen, B.; Ali, M.; Neumann, R.; Ensinger, W.; Knoll, W.; Azzaroni, O. *Nano Lett.* **2009**, 9, 2788.
- (10) Ali, M.; Yameen, B.; Cervera, J.; Ramirez, P.; Neumann, R.; Ensinger, W.; Knoll, W.; Azzaroni, O. *J. Am. Chem. Soc.* **2010**, 132, 8338.
- (11) Ali, M.; Yameen, B.; Neumann, R.; Ensinger, W.; Knoll, W.; Azzaroni, O. *J. Am. Chem. Soc.* **2008**, 130, 16351.
- (12) Hou, X.; Liu, Y. J.; Dong, H.; Yang, F.; Li, L.; Jiang, L. *Adv. Mater.* **2010**, 22, 2440.
- (13) Tian, Y.; Hou, X.; Wen, L. P.; Guo, W.; Song, Y. L.; Sun, H. Z.; Wang, Y. G.; Jiang, L.; Zhu, D. B. *Chem. Commun.* **2010**, 46, 1682.
- (14) Guo, W.; Xia, H. W.; Cao, L. X.; Xia, F.; Wang, S. T.; Zhang, G. Z.; Song, Y. L.; Wang, Y. G.; Jiang, L.; Zhu, D. B. *Adv. Funct. Mater.* **2010**, 20, 3561.
- (15) Yameen, B.; Ali, M.; Neumann, R.; Ensinger, W.; Knoll, W.; Azzaroni, O. *J. Am. Chem. Soc.* **2009**, 131, 2070.
- (16) Yameen, B.; Ali, M.; Neumann, R.; Ensinger, W.; Knoll, W.; Azzaroni, O. *Chem. Commun.* **2010**, 46, 1908.
- (17) Hou, X.; Yang, F.; Li, L.; Song, Y. L.; Jiang, L.; Zhu, D. B. *J. Am. Chem. Soc.* **2010**, 132, 11736.
- (18) Xia, F.; Guo, W.; Mao, Y.; Hou, X.; Xue, J.; Xia, H.; Wang, L.; Song, Y.; Ji, H.; Ouyang, Q.; Wang, Y.; Jiang, L. *J. Am. Chem. Soc.* **2008**, 130, 8345.
- (19) Hou, X.; Guo, W.; Xia, F.; Nie, F. Q.; Dong, H.; Tian, Y.; Wen, L.; Wang, L.; Cao, L.; Yang, Y.; Xue, J.; Song, Y.; Wang, Y.; Liu, D.; Jiang, L. *J. Am. Chem. Soc.* **2009**, 131, 7800.
- (20) Ali, M.; Neumann, R.; Ensinger, W. *ACS Nano* **2010**, 4, 7267.
- (21) Yusko, E. C.; Johnson, J. M.; Majd, S.; Prangkio, P.; Rollings, R. C.; Li, J.; Yang, J.; Mayer, M. *Nat. Nanotechnol.* **2011**, 6, 253.
- (22) Harrell, C. C.; Kohli, P.; Siwy, Z.; Martin, C. R. *J. Am. Chem. Soc.* **2004**, 126, 15646.
- (23) Daiguji, H.; Yang, P. D.; Szeri, A. J.; Majumdar, A. *Nano Lett.* **2004**, 4, 2315.
- (24) van der Heyden, F. H. J.; Bonthuis, D. J.; Stein, D.; Meyer, C.; Dekker, C. *Nano Lett.* **2007**, 7, 1022.
- (25) Howorka, S.; Siwy, Z. *Chem. Soc. Rev.* **2009**, 38, 2360.
- (26) Martin, C. R.; Siwy, Z. *Science* **2007**, 317, 331.
- (27) Zhang, B.; Zhang, Y.; White, H. S. *Anal. Chem.* **2004**, 76, 6229.
- (28) Karnik, R.; Fan, R.; Yue, M.; Li, D.; Yang, P.; Majumdar, A. *Nano Lett.* **2005**, 5, 943.
- (29) Yameen, B.; Kaltbeitzel, A.; Glasser, G.; Langner, A.; Muller, F.; Gosele, U.; Knoll, W.; Azzaroni, O. *ACS Appl. Mater. Interfaces* **2010**, 2, 279.
- (30) Gong, P.; Genzer, J.; Szeleifer, I. *Phys. Rev. Lett.* **2007**, 98.
- (31) Nap, R.; Gong, P.; Szeleifer, I. *J. Polym. Sci., Part B: Polym. Phys.* **2006**, 44, 2638.
- (32) Tagliazucchi, M.; Azzaroni, O.; Szeleifer, I. *J. Am. Chem. Soc.* **2010**, 132, 12404.
- (33) Tagliazucchi, M.; Calvo, E. J.; Szeleifer, I. *J. Phys. Chem. C* **2008**, 112, 458.
- (34) Gong, P.; Wu, T.; Genzer, J.; Szeleifer, I. *Macromolecules* **2007**, 40, 8765.
- (35) Calvo, A.; Yameen, B.; Williams, F. J.; Azzaroni, O.; Soler-Illia, G. *Chem. Commun.* **2009**, 2553.
- (36) Calvo, A.; Fuertes, M. C.; Yameen, B.; Williams, F. J.; Azzaroni, O.; Soler-Illia, G. *Langmuir* **2010**, 26, 5559.
- (37) Lebon, G.; Jou, D.; Casas-Vásquez, J. *Understanding Non-equilibrium Thermodynamics*; Springer-Verlag: Berlin, 2008.
- (38) Prigogine, I. *Introduction to Thermodynamics of Irreversible Processes*; Interscience Publishers: New York, 1955.
- (39) Douglas Frink, L. J.; Thompson, A.; Salinger, A. G. *J. Chem. Phys.* **2000**, 112, 7564.
- (40) Gillespie, D.; Nonner, W.; Eisenberg, R. S. *J. Phys.: Condens. Matter* **2002**, 14, 12129.
- (41) Fang, F.; Satulovsky, J.; Szeleifer, I. *Biophys. J.* **2005**, 89, 1516.
- (42) Fang, F.; Szeleifer, I. *Proc. Natl. Acad. Sci. U.S.A.* **2006**, 103, 5769.
- (43) Satulovsky, J.; Carignano, M. A.; Szeleifer, I. *Proc. Natl. Acad. Sci. U.S.A.* **2000**, 97, 9037.
- (44) Bettolo Marconi, U. M.; Tarazona, P. *J. Phys.: Condens. Matter* **2000**, 12, A413.
- (45) Marconi, U. M. B.; Tarazona, P. *J. Chem. Phys.* **1999**, 110, 8032.
- (46) Fang, F.; Szeleifer, I. *Biophys. J.* **2001**, 80, 2568.
- (47) Peleg, O.; Tagliazucchi, M.; Kröger, M.; Rabin, Y.; Szeleifer, I. *ACS Nano* **2011**, 5, 4737.
- (48) Tagliazucchi, M.; Calvo, E. J.; Szeleifer, I. *Langmuir* **2008**, 24, 2869.
- (49) Carignano, M. A.; Szeleifer, I. *J. Chem. Phys.* **1993**, 98, 5006.
- (50) Longo, G.; Szeleifer, I. *Langmuir* **2005**, 21, 11342.
- (51) Szeleifer, I.; Carignano, M. A. *Adv. Chem. Phys.* **1996**, 96, 165.
- (52) Grosberg, A. Y.; Rabin, Y. *J. Chem. Phys.* **2010**, 133.
- (53) Goldman, D. E. *J. Gen. Physiol.* **1943**, 27, 37.
- (54) Kowalczyk, S. W.; Kapinos, L.; Blosser, T. R.; Magalhães, T.; Van Nies, P.; Lim, R. Y. H.; Dekker, C. *Nat. Nanotechnol.* **2011**, 6, 433.
- (55) Naegeli, R.; Redepenning, J.; Anson, F. C. *J. Phys. Chem.* **1986**, 90, 6227.
- (56) Doblhofer, K.; Vorotyntsev, M. In *Electroactive Polymer Electrochemistry*; Lyons, M. E. G., Ed.; Plenum: New York, 1994; p 375.
- (57) Krapf, D.; Wu, M. Y.; Smeets, R. M. M.; Zandbergen, H. W.; Dekker, C.; Lemay, S. G. *Nano Lett.* **2006**, 6, 105.
- (58) Vlasiouk, I.; Smirnov, S.; Siwy, Z. *Nano Lett.* **2008**, 8, 1978.
- (59) Choi, J. H.; Park, J. S.; Moon, S. H. *J. Colloid Interface Sci.* **2002**, 251, 311.
- (60) Holtzel, A.; Tallarek, U. *J. Sep. Sci.* **2007**, 30, 1398.
- (61) Keyser, U. F.; Koeleman, B. N.; Van Dorp, S.; Krapf, D.; Smeets, R. M. M.; Lemay, S. G.; Dekker, N. H.; Dekker, C. *Nat. Phys.* **2006**, 2, 473.
- (62) Siwy, Z. S.; Howorka, S. *Chem. Soc. Rev.* **2010**, 39, 1115.
- (63) Mussi, V.; Fanzio, P.; Repetto, L.; Firpo, G.; Scaruffi, P.; Stigliani, S.; Tonini, G. P.; Valbusa, U. *Nanotechnology* **2010**, 21.
- (64) Sanchez-Quesada, J.; Saghatelian, A.; Cheley, S.; Bayley, H.; Ghadiri, M. R. *Angew. Chem., Int. Ed.* **2004**, 43, 3063.
- (65) Schoch, R. B.; Han, J. Y.; Renaud, P. *Rev. Mod. Phys.* **2008**, 80, 839.
- (66) Binder, K.; Kreer, T.; Milchev, A. *Soft Matter* **2011**, 7, 7159–7172.
- (67) Pastorino, C.; Binder, K.; Muller, M. *Macromolecules* **2009**, 42, 401.
- (68) Alber, F.; Dokudovskaya, S.; Veenhoff, L. M.; Zhang, W.; Kipper, J.; Devos, D.; Suprpto, A.; Karni-Schmidt, O.; Williams, R.; Chait, B. T.; Sali, A.; Rout, M. P. *Nature* **2007**, 450, 695.
- (69) Peleg, O.; Lim, R. Y. H. *Biol. Chem.* **2010**, 391, 719.